Appl Phys B (2010) 100: 521–533
DOI 10.1007/s00340-010-4112-9

Applied Physics B
Lasers and Optics

Characterization of aerosol plumes in nanosecond laser ablation of molecular solids at atmospheric pressure

T.A. Schmitz · J. Koch · D. Günther · R. Zenobi

Received: 26 August 2009 / Revised version: 6 May 2010 / Published online: 3 July 2010

Abstract Ablation of molecular solids with pulsed ultraviolet lasers at atmospheric pressure is an important process in (bio-)organic mass spectrometry. Of practical importance for analytical sampling and analysis are the plume formation and expansion. Plumes formed by atmospheric-pressure laser ablation of anthracene and 2,5-dihydroxybenzoic acid (2,5-DHB) were studied by light scattering imaging, which showed significant material release in the form of aerosols. The monitored plume expansion dynamics could be fitted to the drag-force model, yielding initial plume velocities of 150 m/s for anthracene and 43 m/s for DHB. While the angle of incidence does not affect the plume direction and propagation, a large dependence of the plume-expansion velocity on the laser pulse energy could be found, which is limited at atmospheric pressure by the onset of plasma shielding. With respect to analytical applications, the efficiency of sampling of the laser ablation products by a capillary could be experimentally visualized.

1 Introduction

Irradiation of materials by laser pulses with high power densities leads to complex light-matter interactions with the eventual ablation of material. This is widely useful in different scientific and engineering disciplines, ranging from material processing applications such as cutting, drilling, pulsed-laser deposition to various analytical applications [1]. For analytical spectroscopy, the use of focused laser irradiation offers the possibility for localized chemical analyses with unmatched ease in terms of sample preparation and sample handling. Depending on the spectroscopic method and the necessary laser irradiance regime, laser induced breakdown spectroscopy (LIBS) [2], laser ablation sampling for inductively coupled plasma mass spectrometry (ICP-MS) [3], laser microprobe mass spectrometry (LMMS) [4, 5] and matrix-assisted laser desorption ionization mass spectrometry (MALDI) [6] are widely used methods for localized chemical or elemental analysis. Typically, laser-based analytical techniques have a very good spatial resolution of 1–100 μm, which can even be increased with special techniques such as using confocal microscopy or scanning near-field optical microscopy [7] for very localized laser illumination.

In MALDI, only the ionized analyte species originating from the laser ablation and ionization process are monitored in a mass analyzer. Since in MALDI very low ion-to-neutral ratios between 10^{-5} and 10^{-3} are typical [8], our design of a mass spectrometer for high-resolution surface analysis is based on sampling neutral ablation products at atmospheric pressure, and guiding them into the ion source of a mass spectrometer by an interface [9].

Analytical laser ablation methods that have been employed and investigated in detail were almost exclusively performed in vacuum. In biological applications, samples often cannot easily be transferred into vacuum. For these cases, pulsed laser ablation of specimens at ambient conditions became particularly interesting. Although laser ablation mass spectrometry at atmospheric pressure (AP) was already demonstrated in 1986 [10], it was only with the advent of AP-MALDI in 2000 [11] that laser ablation at atmospheric pressure became a standard technique for bioanalytical mass spectrometry and even imaging. Despite the wide use of laser ablation in mass spectrometry, our knowl-

T.A. Schmitz · J. Koch · D. Günther · R. Zenobi (✉)
Department of Chemistry and Applied Biosciences, ETH Zürich, 8093 Zürich, Switzerland
e-mail: zenobi@org.chem.ethz.ch
Fax: +41-44-6321292

edge of the ablation processes is not yet complete [12], although the overall processes governing laser ablation [13, 14], laser ionization [15] or MALDI [8, 16] have been extensively examined.

The physical processes which govern laser ablation plume formation and expansion have been studied theoretically [17, 18], with simulations [19–21], as well as experimentally. Experimental work that covers laser ablation at atmospheric pressure is quite scarce [22–25]; while some papers are only dealing with pressures in the millibar range [24], others deal with typical gas atmospheres used in laser ablation inductively coupled plasma mass spectrometry (LA-ICP-MS) [23, 25]. In terms of materials, many studies have looked at the interaction with metallic substrates, with silicon or with ceramic materials which are typical aerosols for ICP-MS [26]. To our knowledge, only very limited research on the plume formation and propagation of atmospheric-pressure laser ablation in air of molecular van der Waals solids has been performed: one such case is work that investigated water rich biological targets [27–29], which exhibit significantly different ablation phenomena due to the violent boiling effects. Two publications by Yeung et al. have appeared in the mid-90s [30, 31]. These workers characterized the evolution of absorption and gas phase fluorescence of MALDI matrix and analyte in a plume at atmospheric pressure. Atmospheric pressure was chosen for practical experimental reasons; AP-MALDI as an analytical technique did not yet exist at that time.

To better understand current practical limitations in ambient pressure laser ablation mass spectrometry, a characterization of the plume formation and a better understanding of how to efficiently sample material from the plume is necessary. We therefore chose a high-speed imaging method, which allows the visualization of laser ablation aerosol over a large range of particle sizes and over extended time, since laser ablation sampling occurs at a much larger timescale than the laser pulse. Phase transitions resulting in material ejection, particle formation, and fast expansion cover several orders of magnitude in time, but also require high temporal resolution (∼nanoseconds) to monitor fast, transient phenomena such as shockwave propagation. To obtain information on plume and shockwave formation, as well as their time evolution, laser ablation processes have been studied using shadowgraphy, which is the method of choice for imaging such ultrafast phenomena [22–25]. When imaging particles, however, shadowgraphy suffers from limited contrast for very small particles or low plume densities. Unless low coherence lasers or incoherent light sources are used, the image quality may be also affected by fringes due to changes in the refractive index of air. While the latter effect can be useful to obtain information on temperature and pressure changes in air, it will lead to an even inferior image quality when imaging aerosols. The ultrafast processes in the very beginning of laser ablation were not a focus of this work. Therefore, laser induced light scattering was chosen instead. As shown previously [32, 33], this method is very suitable for observing aerosol plumes generated from laser ablation with high spatial and temporal resolution. Compared to other imaging methods for fast processes such as laser-based shadowgraphy, light scattering imaging offers extremely good contrast and superior image quality for imaging aerosol particles; since only a small region of the generated laser ablation plume is intersected by the illumination laser, a quasi-2D image slice can be acquired instead of a projection of the 3D plume onto a 2D imaging plane. As gaseous ablation products or shock and sound waves cannot be visualized by light scattering, the term “plume” therefore refers to the aerosolized ablation products (solid particles) in the context of this paper.

The aim of this paper is to give new experimental insight into the characteristics of atmospheric-pressure laser ablation of molecular solids. Fundamental questions in analytical laser ablation sampling are: Are mostly vaporized atoms and clusters or, rather, a large fraction of particles formed by the ablation process (too large particles may not be amenable to ionization)? How does a laser ablation plume expand in space and time? What is the stopping distance of the laser ablation plume and what are the consequences for analytical sampling and the overall instrumental design? To understand the basic processes of laser ablation at ambient conditions, the plume expansion is investigated in this work, with particular attention to the possible implications for analytical sampling.

2 Experimental setup

2.1 Chemicals and samples for laser ablation

Anthracene was used as a model compound for laser ablation of organic molecular solids in this study; due to its good absorption in the UV (molar absorption coefficient: $\log \varepsilon = 3.92$ for $\lambda = 357$ nm) and low melting point (218°C) it is well suited for laser ablation studies in the UV. Additionally, 2,5-dihydroxybenzoic acid (2,5-DHB), which is a commonly used MALDI matrix, was used for comparison. Both chemicals were bought in the highest available quality from commercial suppliers (Fluka AG, Buchs, Switzerland; Acros Organics, Geel, Belgium) and were used without further purification. From the crystals or powder of both solid compounds very flat pellets with a thickness of several millimeters were produced as laser ablation targets in a hydraulic IR press by applying a load of 10 tons for 5–10 minutes.

2.2 Laser ablation

Laser ablation was performed at atmospheric pressure using a nitrogen laser (337 nm wavelength, pulse width 4 ns FWHM, pulse energy 235 μJ; LSI VSL-337ND, Spectra Physics, Mountain View CA, USA), a source that is often used for UV-MALDI. After attenuation with a variable metallic neutral density filter, the light was focused with a plano-convex fused-silica UV lens ($f = 30$ mm) from above onto the surface of the target, yielding a spot size of 100–150 μm. Unless otherwise noted, the laser energy was 170 μJ/pulse, corresponding to a fluence of ∼1.4 J/cm^2 and an irradiance of $\sim 3.5 \times 10^8$ W/cm^2 (for an estimated average spot size of 125 μm). The sample platform was mounted on a lab jack for adjustment of the z-position. Sample tilt could be adjusted by a goniometer, while sample translation in x- and y-direction could be performed by a mechanical micrometer translation stage. Unless otherwise noted, the sample was moved to a new position for every laser ablation experiment.

2.3 Visualization of the ablation plume

Laser-induced light scattering was chosen for visualizing the dynamics of the plumes and ablation products. A setup similar to the one used in a study of aerosols generated by nano- and femtosecond laser ablation in closed ablation cells [32] was employed (see Fig. 1). A frequency-doubled Nd:YAG laser (532 nm wavelength, pulse width 4–6 ns; Minilite-10, Continuum, Santa Clara CA, USA) was used for pulsed illumination. Typically, a pulse energy of 6–8 mJ was employed. A periscope equipped with dichroic mirrors changed the laser light polarization from horizontal to vertical. The light first passed through a horizontal slit made from 2 sharp knife blades mounted on micrometer positioners and then through a vertical slit (entrance slit scavenged from an old SPEX 500M spectrometer) to form a sheet of light with a height of ∼4–8 mm and a width of 50–200 μm, which intersects the region of ablation. By using vertically polarized laser light for illumination and collecting the scattered light at an angle of 90°, the full particle size range from Rayleigh, Debye and Mie scattering is accessible [34].

The scattered light was imaged parallel to the incoming light sheet by a high-resolution monochrome CCD camera (1600 × 1200 pixel, greyscale, 10-bit dynamic range; CV-M2CL, Jai A/S, Glostrup, Denmark), which is equipped with a macro zoom objective (0.8–4.0× zoom with integrated iris; Linos, Göttingen, Germany). The camera was mounted on an assembly that could be accurately moved in all three directions using micro positioning translation stages to control the field of view and the focus of the camera system.

Timing and triggering of the experimental setup was controlled by a four-channel digital delay/pulse-generator (5 ps delay resolution, 50 ps rms jitter; DG535, Stanford Research Systems Inc., Sunnyvale CA, USA), which was used as master clock to trigger the camera exposure, the nitrogen ablation laser and the Nd:YAG illumination laser. At $t = 0$ the CCD camera was triggered, which was programmed to run in edge pre-selected burst trigger mode, taking five consecutives exposures with a burst shutter of 2.81 ms for the first exposure and 34 ms for subsequent exposures #2–#5. The burst images of the CCD camera were acquired using proprietary software (CVB Tools; Stemmer Imaging GmbH, Puchheim, Germany) and saved manually after each experiment. Except for very long Δt values, only the first exposure was saved as it contained both the emission from the initial laser ablation event (plasma emission, if formed) and from the scattered laser light; the exposure time chosen for the first burst was optimized to allow the experiment to be run at normal laboratory lighting without an appreciable increase in the imaging background.

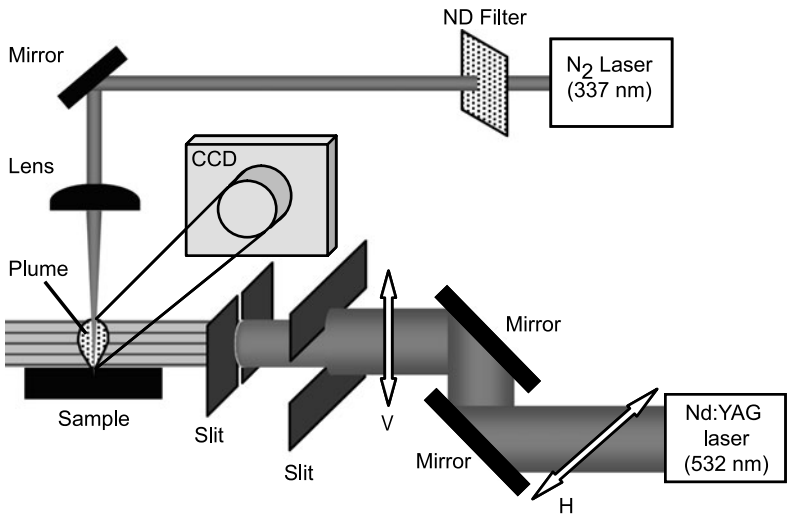

Fig. 1 Experimental setup for the visualization of laser ablation plumes at atmospheric pressure by laser-induced scattering

By changing the delay between triggering the nitrogen laser for ablation and the Q-switch trigger for the Nd:YAG illumination laser, the effective exposure delay (Δt) for laser induced scattering imaging could be set. By triggering the flashlamp of the Nd:YAG laser an arbitrary time before the Q-switch trigger, the laser intensity could be adjusted for optimum imaging conditions (typical Q-switch delay of 200 µs, yielding 8 mJ/pulse). The effective optical delay when triggering the nitrogen laser and the Q-switch of the Nd:YAG at the same time was found to be 120 ns, but since the Δt used in this study were in the microsecond time range (0–30,000 µs), all delays reported will refer to the uncorrected delay times set on the DDG.

2.4 Analytical sampling of laser ablation plumes

To observe laser plumes being sampled, a membrane pump with a maximum pumping speed of 1.6 m^3/h (Büchi Vac V-500; Büchi AG, Flawil, Switzerland) was used with different capillaries/sampling tubes (i.d. 510 µm; 1.0 mm and 2.1 mm). Air flow rates were controlled and measured using a mechanical direct reading flow meter (Uniflux LVB 0.5–16 l/min, Uniflux LVB 2–36 l/min; Influx Measurements Ltd., Alresford, UK). The capillaries were positioned in the illumination axis using an x–y–z micro positioning assembly; care was taken to limit the amount of scattered light from the capillaries (by blackening the capillaries and blocking any scattered light to the CCD).

2.5 Data processing and evaluation

Images were processed using a commercial image editing software (Paint Shop Pro XI; Corel Corporation, Ottawa ON, Canada); all pictures were cropped to the desired field of view; where necessary contrast and dynamic range were optimized. Measurement of plume sizes, angles etc. were performed manually and processed with standard software. For size calibration, a standard electron microscopy grid (Maxtaform 50 Mesh; Pyser-SGI Ltd., Edenbridge, UK) and a 1 mm ruler disc with 0.01 mm/0.05 mm/0.10 mm markings (PELCO No. 630; Ted Pella Inc., Redding CA, USA) was used. We define the "plume size" as the radius between the point of laser ablation and the outmost edge of the plume.

3 Results and discussion

3.1 Plume propagation: general aspects

The propagation of the plume generated by laser ablation of an anthracene pellet at atmospheric pressure was investigated using the described laser-induced light scattering method for delay times (Δt) from 0–30,000 µs after irradiation by the ablation laser. During laser ablation, the material in the laser focus is heated and removed by vaporization and melt ejection [35]. Ejection of molten material is possible both by boiling as well as by the recoil pressure of the back-reflected internal shock wave on the molten liquid [36]; the latter phenomenon only exists in atmospheric-pressure laser ablation, since in vacuum no internal or external shock waves can be formed. Particles in atmospheric-pressure laser ablation are also formed by condensation of supersaturated vapor in the ablation plume [37].

Figure 2 shows a representative image series of the propagation behavior of the anthracene laser ablation plume. Already 5 µs after the initial ablation laser shot, the solid laser ablation products are distinctively visible; at earlier times there were few particles being ejected, and these cannot unambiguously be observed since the light scattered towards the camera was superimposed by plasma emission. With time, the plume expands straight in z-direction with a "mushroom" cloud-like appearance, given by a visible vortex ring at the plume head and a faint tail ("stem"), which exhibits irregular patterns. The images demonstrate that a large part of the spatial expansion over time occurs in the first 100 µs, while afterwards the expansion becomes progressively slower. For delays greater than 800 µs, the plume top is no longer visible due to a forward/backward movement out of the plane of illumination (cf. picture at 1,000 µs and 20,000 µs; even with a larger field-of-view than actually shown, the plume head was not visible for that reason).

Due to the imaging method applied, every image frame originates from an individual laser ablation experiment and not from consecutive imaging of the same event. Nevertheless, we note that the evolution of the laser ablation plume is sufficiently reproducible—even at the conditions encountered for ambient laser ablation in a standard laboratory environment.

Ablation experiments were performed with nearly forty different Δt values, with two to four replicates for each delay (except for delays >6,000 µs). For the numerical evaluation of the plume propagation, the radius of the plume was measured for every acquisition until $\Delta t = 800$ µs, from the ablation spot on the surface to the outmost edge of the plume. Figure 3 shows a plot of the plume radius versus delay time Δt. The very fast initial expansion, followed by progressively slower expansion, as seen in Fig. 2 is consistent with the numerical values.

A classical drag-force model was fitted to the experimental data (see Fig. 2). In the drag-force model, the products ejected by laser ablation experience a viscous force proportional to their velocity through the background gas [38]:

$$v(t) = v_0 \exp(-\beta t) = v_0 - \beta r(t) \quad (1)$$

$$r(t) = (v_0/\beta)\left[1 - \exp(-\beta t)\right] \quad (2)$$

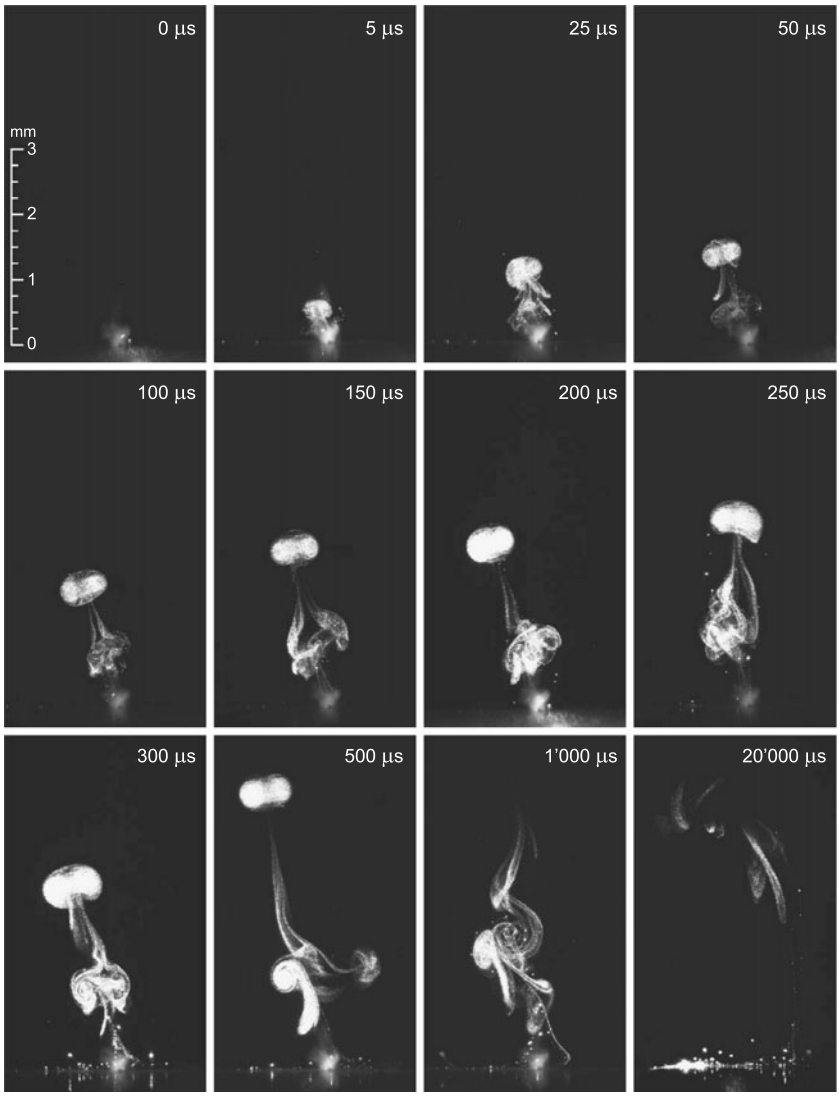

Fig. 2 Expansion of plume formed by laser ablation of anthracene at atmospheric pressure; for every image the delay Δt between laser ablation and photographic "snapshot" is noted

where the velocity (v) and position (r) at a given time are only dependent on the initial velocity v_0 and a slowing coefficient β, the latter being dependent on the physical properties of the ejected particles and the surrounding atmosphere. Ultimately, the plume reaches a stopping distance at v_0/β. This is in sharp contrast to laser ablation in vacuum, where the initial velocity v_0 is conserved in the absence of collisions with either residual gas molecules or walls, resulting in an unlimited free expansion of the plume front with $r(t) \propto t$ [24, 39, 40]. At higher pressures, the free expansion relationship is only true for the very initial phase within a few tens of ns. Then, the supersonic expansion of a laser ablation plume into a background gas will result in shock wave formation and propagation, which can be described using a blast wave, or so-called point-blast model [41], similar to the Sedov–Taylor solution [42, 43] for conventional spherical explosions in a homogeneous atmosphere, with $r(t) = \xi_0 \ (E_0/\rho_{\mathrm{Gas}})^{1/5} t^{2/5}$ [44]. As discussed and experimentally demonstrated, this model is applicable in laser ablation for pressures higher than 1–15 mbar during the initial expansion period (ns–1 µs) [24, 44].

While Geohegan noted a good agreement first with the drag-force model and then, after an initial expansion, a better agreement with the shock model, this only seems to hold true for very low "atmospheric" pressures (mTorr) and only on the timescale of a few microseconds, as long as the shockwave persists [38]. In the recent literature, Amoruso et al. proposed a gas-dynamic model based on the work of Predtechensky and Mayorov as an alternative to the point-blast model, to describe the expansion of a shockwave for typical pressures used in pulsed laser deposition experiments in the pressure regime between 0.01 and 0.2 mbar [45]. As opposed to the point-blast model, this approach is characterized by an initial free expansion and finite plume stopping. At higher pressures and on the microsecond time scale, i.e. for the conditions considered here, the drag-

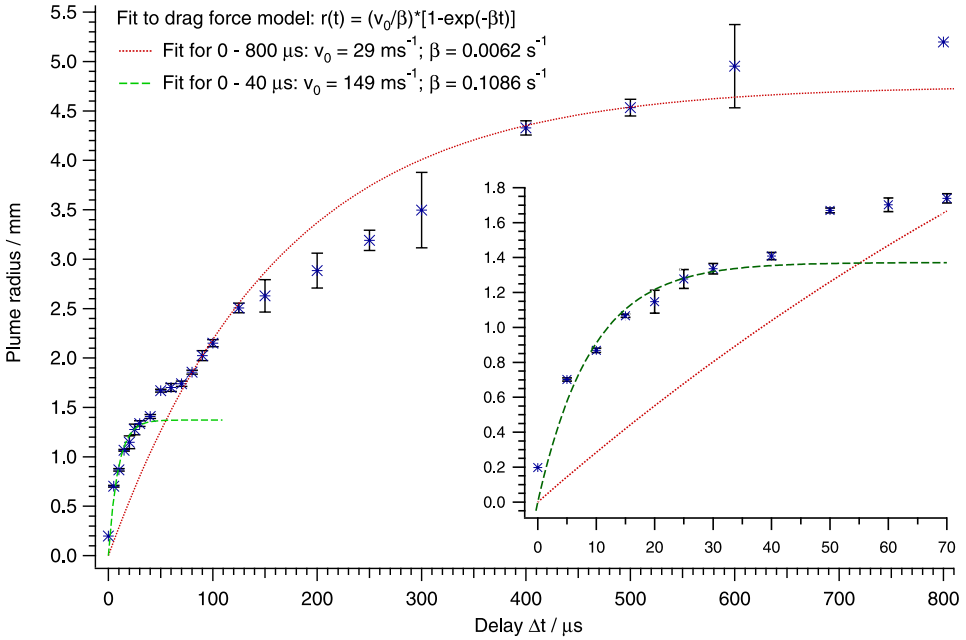

Fig. 3 Plot of the experimentally determined plume radius $r(t)$ versus delay time Δt (from experimental series depicted in Fig. 2). The drag-force model does not fit the experimental data over the entire time range correctly; therefore a second fit over an initial period of 40 µs was performed. The *inset* shows a close-up of the initial phase

force model is giving a good description of the experimentally observed plume expansion [23, 24, 32, 39, 46].

In our case, the drag-force model does not fit the entire time range monitored, as it is evident from Fig. 3. The expansion appears to happen in two different phases: The initial phase from 0–40 µs fits the drag-force model very well, with an initial velocity v_0 of ∼150 m/s. Instead of stopping at the theoretical stopping distance $v_0/\beta = 1.37$ mm (calculated from (2) with fit parameters of Fig. 3), the plume further expands without reaching a defined stopping distance, at least on the time scale in our experiments. While we cannot offer a model for the further expansion of the plume, we assume that in the second phase, the inconsistency of observed and calculated plume expansion arises from ambient flows as a result of convection, airflows from the laboratory venting system and, to a smaller extent particle diffusion, which carries the aerosol particles further. According to Stoke's law it is not unlikely for very small particles below a diameter of 5 µm to remain suspended for extended periods in ambient air. Prolonged suspension of small particles in laser ablation was already demonstrated in previous work [32].

From the data shown in Figs. 2 and 3, the momentary velocity of the particles at the plume front was estimated for each time step by manual stepwise derivation (dividing the distance travelled by the elapsed time between two data points). The resulting velocities are plotted in Fig. 4 as a function of Δt. The data were fitted to (1), which describes the evolution of the speed of the ablation products. Although the resulting velocity at early Δt values has to be considered as a very coarse estimate, the fit to the drag-force model seems valid. As Fig. 4 demonstrates, at $\Delta t = 150$ µs at the latest, the expansion velocity has almost vanished; only a residual velocity of a few meters per second seem to remain, as already mentioned.

In a laser ablation set-up used for mass spectrometry, the sample may be mounted on a tilted stage with the incoming ablation laser off the surface normal. In LIBS, it is known that the atomic emission observed from ejected sample material is always perpendicular to the sample surface [47]. To confirm that this holds true for the expansion of a particle plume in general, the influence of the angle of incidence on the direction of plume expansion was studied with our scattering imaging method. As can be seen from Fig. 5, the laser ablation plume always expands in near normal direction with respect to the surface, independently of the surface tilt angle and the angle of incidence for the ablation laser. We note that a different behavior is expected for repeated laser ablation at the same spot, when material is ejected from a deepening crater as opposed to a shallow pool of melt: in this case, the ejection of sample is thought to occur along the axis of the crater, which will roughly trace the axis of the incident laser beam.

3.2 Influence of laser pulse energy on plume propagation

Besides wavelength and pulse duration, the laser pulse energy is one of the most important parameters in laser ablation. The influence of the energy on the plume propagation was investigated for ablation of anthracene by measuring the plume radius r at two distinct times, $\Delta t = 50$ µs and 200 µs, while varying the incoming laser power. The dependence of the resulting plume radius on the pulse energy used for laser ablation can be seen in Fig. 6. As discussed in Sect. 3.1,

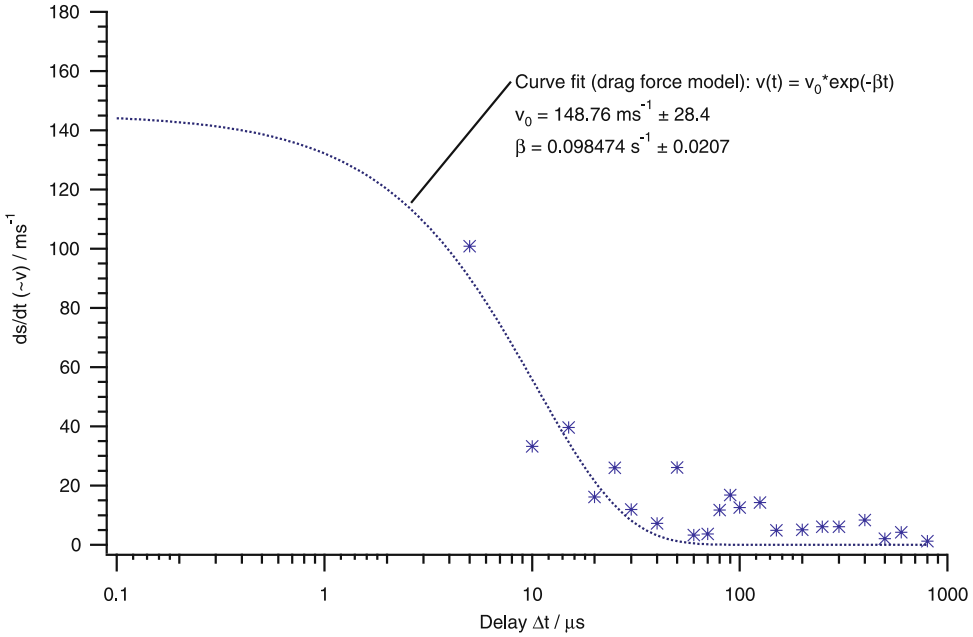

Fig. 4 Plot of the velocity versus delay time Δt (data derived from Fig. 3), including fit to the drag-force model

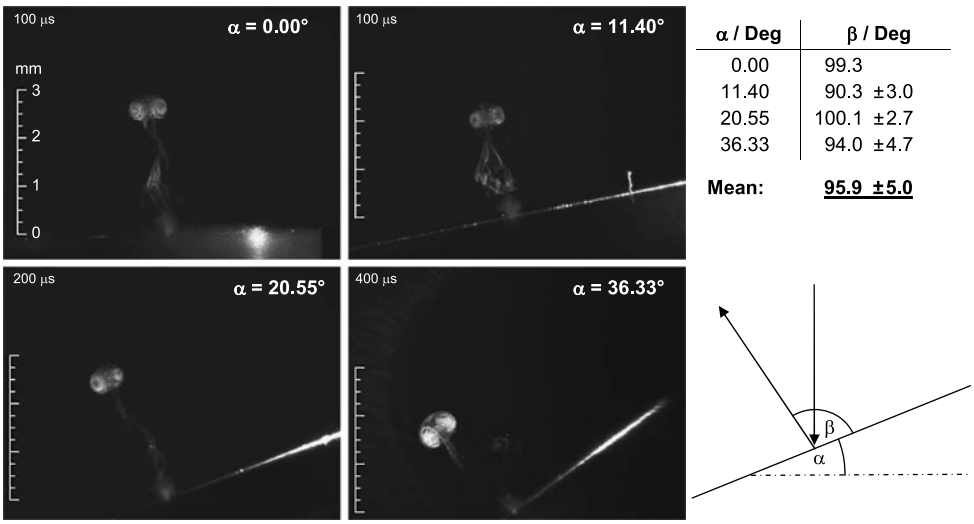

Fig. 5 Plume expansion for different angles of incidence of the ablation laser

the propagation of the laser ablation plume in the drag-force model depends solely on the initial velocity v_o and the slowing coefficient β. Since v_o can be deducted from the initial kinetic energy $E_{0,\mathrm{kin}}$ and the mass of the ablation products, one might expect a direct relationship between r and the incoming ablation laser energy E_{laser} given the laws of energy conservation and a very basic model of laser ablation:

$$E_{\mathrm{laser}} - E_{\mathrm{refl}} = E_{\mathrm{heat}} + E_{\mathrm{melt}} + E_{\mathrm{evap}} + E_{0,\mathrm{kin}} + E_{0,\mathrm{thermal}} = E_{\mathrm{threshold}} + E_0 \quad (3)$$

For a higher incoming laser energy, a higher initial velocity v_o and thus a greater r at a given Δt would therefore be expected. As Fig. 6 shows, this is true until a plateau is reached. For input laser energies of 72 µJ/pulse and larger, we found no further increase in plume size and initial velocity, respectively. This phenomenon can be explained by the onset of so-called plasma shielding [48] of the incoming laser light, which is dependent both on the background gas pressure as well as on its ionization potential [49, 50]. Obviously the effective energy available for conversion into kinetic energy in the laser ablation process remains constant as soon as the plateau value of 72 µJ/pulse, equal to a fluence of ~0.6 J/cm^2 and an irradiance of $\sim 1.5 \times 10^8$ W/cm^2, is reached. Further inspection of the image frames (not shown here) confirms that for energies ≥72 µJ/pulse, an intense plasma is being formed above the irradiated area. The general plume shape was found to be very similar for all laser energies

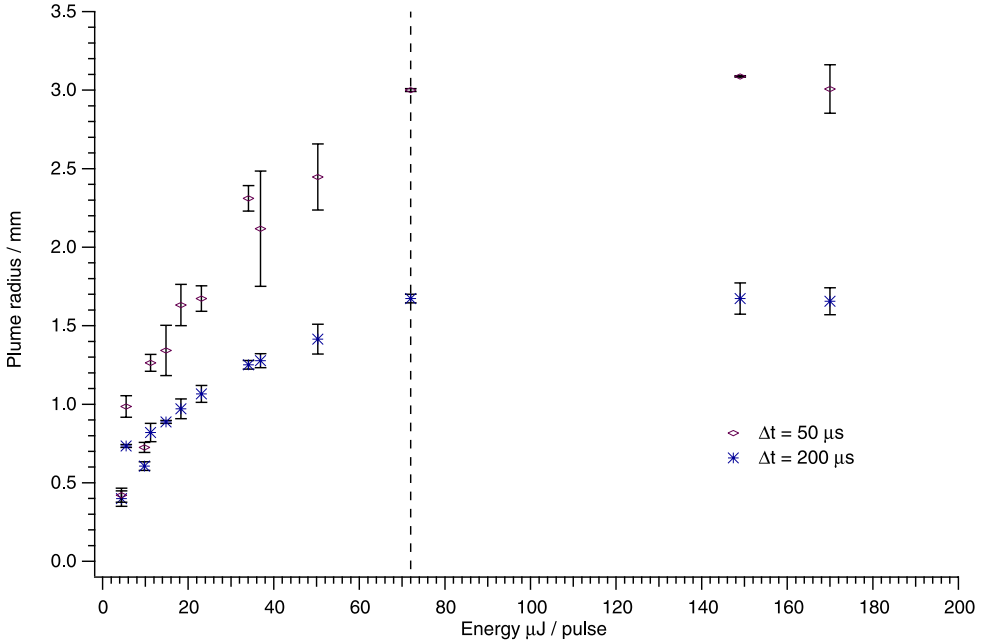

Fig. 6 Experimentally determined influence of the laser energy on expansion velocity; for two different delay time Δt, the plume radius is plotted as a function of the laser energy per pulse (4.4–170 µJ/pulse, corresponding to a fluence of ~0.04–1.4 J/cm^2)

examined in this study (ablation wavelength 337 nm; pulse width 4 ns FWHM). It is therefore evident that any additional energy is being absorbed in the plasma and will neither be available for ablation of additional material nor contribute to the speed of plume propagation. Since plasma shielding is absent in vacuum laser ablation, higher background pressures should therefore lead to limited laser ablation yields at higher laser energies, as reported for the ablation of metals at air pressures from 0–1000 mbar [49]. On the other hand, laser ablation at increased background pressures might benefit from additional material ejection caused by the recoil pressure of the internal shock wave on molten material; a phenomenon not present in vacuum, either.

3.3 Plume formation in consecutive laser ablation (pulse train at the same spot)

While all other experiments in this work were performed at pristine ablation sites, the influence of repeated laser ablation on the same spot on the plume formation was qualitatively assessed. Ablation was performed on an anthracene sample at a fixed sample position using a nitrogen laser running freely with a repetition rate of 10 Hz. A selection of 6 acquired image frames is displayed in Fig. 7. For the first twelve shots, no difference in plume shape can be observed. From this point on, increasingly irregular plumes are formed for every consecutive laser ablation event. At the end of the series, the plumes lack the typical vortex head observable in every other experiment performed in this work. The reason for the absence of vortex formation and the observed chaotic behavior is unknown yet, but might a result of phase changes in the sample. These could lead to different physical properties of the re-crystallized material on the sample surface, rim and crater formation. While the first would imply fundamental changes of the laser-matter interaction, the latter would lead to different characteristics regarding the amount of material removed and the material ejection compared to a flat surface.

3.4 Plume formation and dynamics in laser ablation of DHB

For comparison with the results obtained by laser ablation of anthracene, plume formation and dynamics for DHB, a common MALDI matrix, are presented in Figs. 8 and 9. Although the ablation plumes formed of DHB do not exhibit the distinct “mushroom” shape as the experiments on anthracene (cf. Fig. 2), some similarity still exists. Evident from both the graphical (Fig. 8) and the numerical results (Fig. 9), the propagation of the plume formed off DHB is significantly slower than for anthracene. This is attributed to its different physical properties such as the optical absorption (greater for DHB than for anthracene at 337 nm), resulting in a smaller laser penetration depth, and its melting point (205°C, slightly lower than for anthracene). Due to the slow velocity, plumes can be observed over a much longer time (1500 µs) before moving out of the plane of illumination. A good fit with the drag-force model is also possible in the high kinetic energy stage of the expansion, yielding an initial velocity v_0 of 43 m/s, over 3 times less than for anthracene. Furthermore, the region which accurately fits the drag-force model covers a larger Δt range (until 200 µs) than for anthracene. The influence of the laser energy on plume propagation and the occurrence of the plasma shielding effect

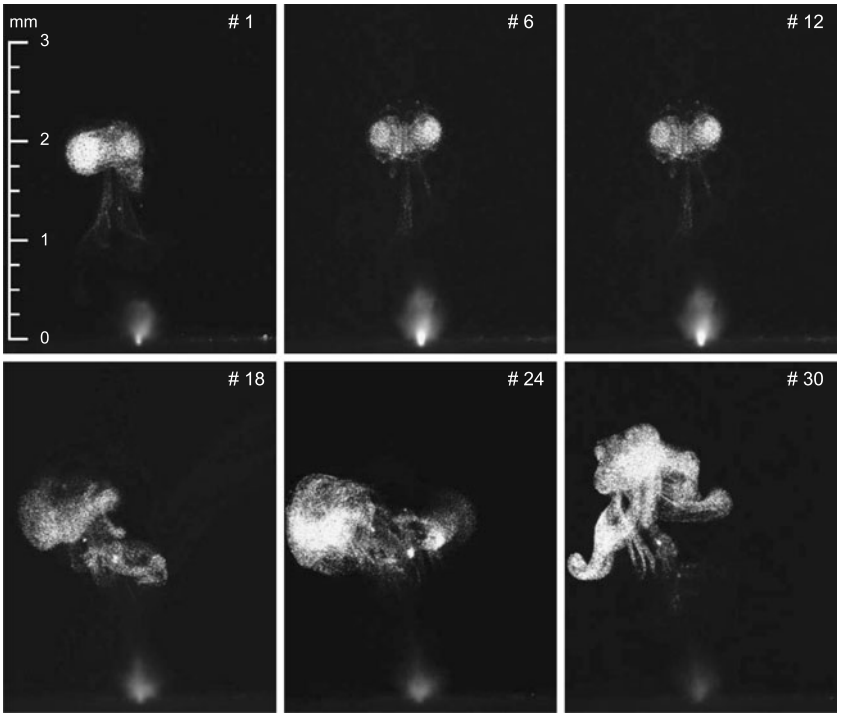

Fig. 7 Plume formation and expansion for repeated laser ablation on the same location; a selection of 6 images representative for the progressing deviation from "one-shot" laser ablation is shown (shot number indicated)

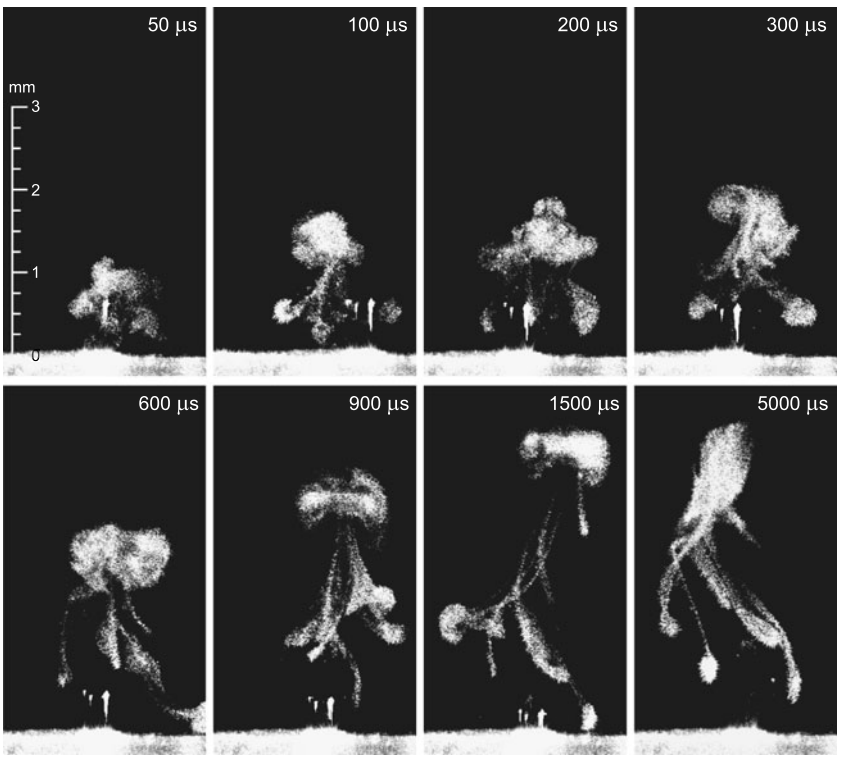

Fig. 8 Expansion of plume formed by laser ablation of 2,5-DHB at atmospheric pressure (laser energy 149 µJ/pulse, corresponding to a fluence of ~1.2 J/cm^2)

can also be seen in Fig. 9, which shows for ablation with an energy of 149 µJ/pulse (fluence ~1.2 J/cm^2; irradiance ~3.0 × 10^8 W/cm^2) or 170 µJ/pulse (fluence ~1.4 J/cm^2; irradiance ~3.5 × 10^8 W/cm^2) no pronounced difference in plume radius at Δt values below 400 µs and above 1000 µs. It is assumed that also for Δt values between 400 µs and 1000 µs no significant difference between the two energies would exist in the case of repeat measurements.

Although differences in laser ablation of anthracene and DHB exist, mainly due to the varying v_0 among the two materials, both showed similar features in the expansion. Therefore we conclude that DHB and anthracene are suf-

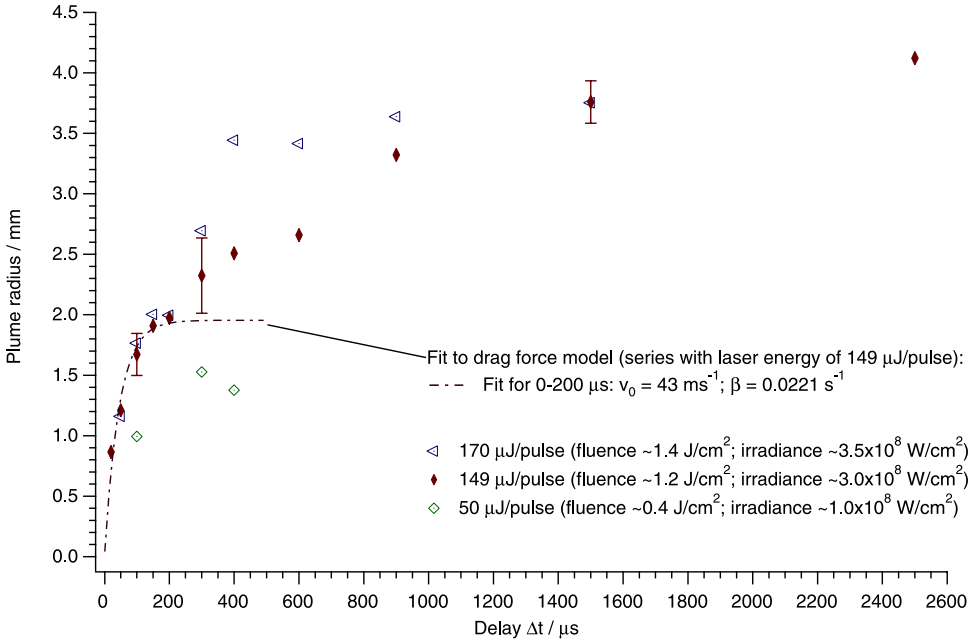

Fig. 9 Plot of the experimentally determined plume radius $r(t)$ versus delay time Δt for 2,5-DHB (from experimental series depicted in Fig. 8) for three different laser energies. For the series with an energy of 149 µJ/pulse (fluence ~1.2 J/cm^2), the drag-force model was fitted to the initial expansion region (0–200 µs)

ficiently similar to allow the general experimental results obtained in this work with anthracene to be transferred to DHB.

3.5 Plume sampling for analytical applications

The sampling efficiency for laser ablation products in expanding plumes was investigated using different experimental configurations. The most important parameters were found to be the dimension and positioning of the sampling capillary, as well as the gas flow through it, in relation to the speed of the laser ablation products.

As examples, Fig. 10a shows both an example of plume expansion with a capillary (i.d. 1.0 mm) held in position without any flow through it and, in comparison, the same capillary with a constant flow. The resulting plume is pictured for different Δt values. For this configuration, it is demonstrated that efficient plume sampling starts between 150 µs and 200 µs after ablation. After 600 µs, the plume is completely sampled. Therefore, we conclude that the vertical expansion speed of the ablation products needs to be sufficiently small to exert an effective "drag" force (efficient suction) towards the sampling capillary, otherwise they cannot be captured. This is especially evident when considering the situation after 200 µs, where the fast "head" of the plume expanded first to a vertical height of 3.2 mm, to be efficiently sampled only in the interval from 200 µs to 300 µs. This has consequences for the timing of ionization in a mass spectrometer as well as for the maximum laser ablation repetition rate in MS imaging applications attainable without mixing of sample plumes released from consecutive events. From this experiment, the Δt value for all further experiments was chosen to be 600 µs.

Figure 10b illustrates the influence of the flow for a given position at $\Delta t = 600$ µs using a capillary with an internal diameter of 1.0 mm as in Fig. 10a. The capillary was positioned with an X-offset of 1.66 mm, Z-offset of 2.34 mm and a radial distance of 2.88 mm from the spot of laser ablation (to the center of the capillary orifice). For this position, the plume starts to be weakly sampled only at a flow of 10 l/min (linear flow velocity of 212 m/s at the capillary inlet). A partial sampling was attained at 11 l/min (233 m/s) and complete sampling at 12.5 l/min (265 m/s), which is already near the upper flow limit for this configuration. For a given position of the capillary, complete sampling of the plume was found to be very sensitive to the absolute flow or flow velocity; below some critical value, there will be no or only very inefficient material sampling.

Figure 10c shows a different series for a constant flow of 7.5 l/min (159 m/s). The capillary was moved stepwise along the x-axis towards the laser ablation site. At an X-offset of 1.67 mm from the spot to the center of the capillary orifice, sampling starts (Pos. 1, tail slightly sampled). Substantial sampling from the plume tail starts at an X-offset of 0.60 mm (Pos. 3) and full sampling at 0.23 mm (Pos. 7; note the small difference to the previous position #6 of only 115 µm). For efficient plume sampling, the horizontal distance between the ablation spot and the capillary is therefore much smaller than the inner diameter of the capillary itself (for the flow rate used here). Comparison of the situation of Fig. 10b (1.66 mm sampling distance for 12.5 l/min) with 10 c (0.23 mm sampling distance for 7.5 l/min) shows an increase in sampling distance for higher flow velocities (265 m/s instead of 159 m/s). It shall be noted that an increase in sampling distance by using higher pumping capac-

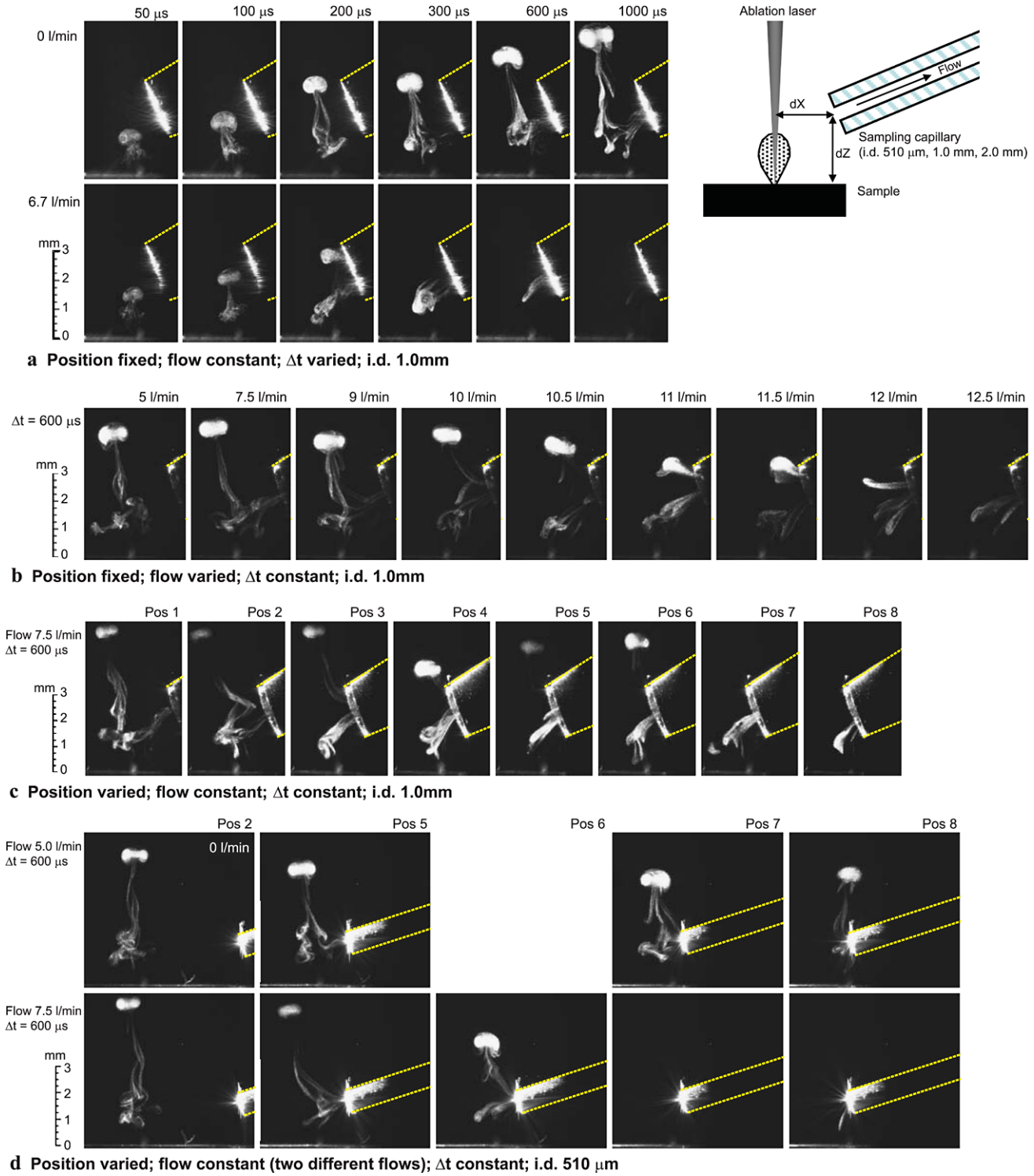

Fig. 10 Plume sampling experiments under different experimental conditions (see text). A schematic representation of the setup is shown in the *top right* corner. *Dashed lines* indicated the outline of the sampling capillary in every frame

ities, resulting in higher flow rates, is only possible as long as the conditions for choked flow are not yet reached.

In Fig. 10d the influence of capillary position for two different flows and a capillary with an inner diameter of 510 µm is shown. A full plume sampling can only be achieved with a flow of ≥7.5 l/min (612 m/s), even when the capillary inlet is positioned close to the axis of laser ablation (Pos 8). Weak sampling of the tail at a flow of 7.5 l/min begins at

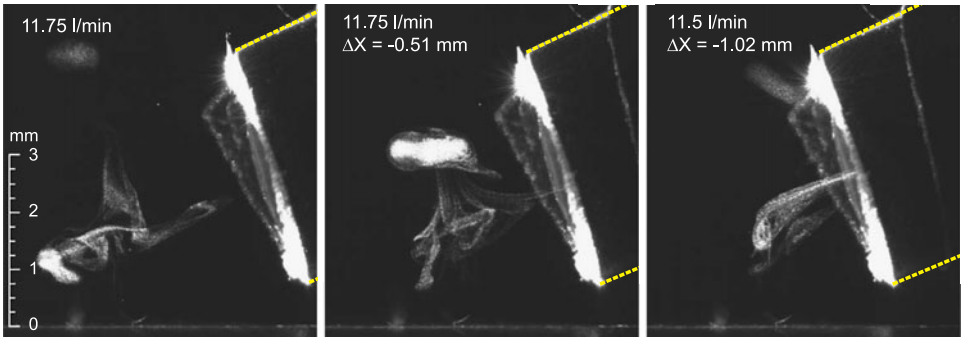

Fig. 11 Plume sampling experiment with a capillary i.d. of 2.0 mm for changed X-offsets and a fixed flow of 11.75 l/min (the third picture yields the same result for 11.5 l/min as for 11.75 l/min). The outline of the sampling capillary is represented by *dashed lines*. The schematic of the experimental setup is identical to that shown in Fig. 10

an X-offset of 1.10 mm (Pos 5), partial sampling at 870 µm (Pos 6), and full sampling at 400 µm (Pos 7). At the last position, a reduced flow of 5.0 l/min (408 m/s) was found to result in slight sampling, highlighting that especially for small capillaries the boundaries for successful plume sampling are quite narrow. The reduction in capillary size by a factor 2 compared to the capillary used in Fig. 10a–c allowed for a nearly twofold increase in sampling distance for the same absolute flow. This is the result of the roughly 4 times higher flow velocity, due to the smaller capillary size.

For a tube with an inner diameter of 2.1 mm, the same experiment can be seen in Fig. 11. For a fixed flow of 11.75 l/min (57 m/s), sampling starts at an X-offset of 2.94 mm whereas full plume sampling is reached at 2.44 mm. Compared to the situation shown in Fig. 10a–c, the doubled capillary diameter allows full sampling of the plume at 1.2 times its inner diameter (instead of 1/4 of i.d.), for a 50% increase in absolute flow.

To obtain an answer to the practical question about which sampling geometry and conditions are most adequate to efficiently sample laser ablation aerosols, a detailed theoretical modeling and/or computational fluid dynamics simulations would be necessary. However, the goal of the experiments shown here was to demonstrate that sampling efficiency can be monitored with the presented imaging setup and to give guidelines for the crucial parameters, flow and position versus capillary size, for a few configurations. It shall also be noted that complete aerosol sampling without the usage of closed ablation cells, which are commonly applied in ICP-MS, could be demonstrated.

4 Conclusions

The characteristics of aerosol plumes formed by atmospheric-pressure laser ablation of molecular van der Waals solids were studied by light scattering imaging. The plume-expansion dynamics of anthracene and DHB could be followed and fitted in the initial phase to a drag-force model. The influence of experimental parameters such as the laser pulse energy or angle of incidence of the ablation beam on the plume-expansion was studied. The particle velocities at the beginning and during plume expansion were found to play a significant role with respect to aerosol sampling for analytical purposes. It could be experimentally demonstrated that comprehensive sampling critically depends on the right choice of flow velocity, capillary diameter and distance. Thus, the work presented contributes valuable insight on the laser ablation of molecular solids at atmospheric pressure and practical guidelines on the sampling of laser-produced aerosols. Ultimately, this will be of help when designing laser ablation-based setups for mass spectrometry.

Acknowledgements Technical support from H. Benz (electronics) and C. Bärtschi/K. Baumgartner/R. Dreier (mechanical workshop) is gratefully acknowledged.

References

1. D. Bäuerle, *Laser Processing and Chemistry*, 3rd edn. (Springer, Berlin, 2000)
2. A.W. Miziolek, *Laser-induced Breakdown Spectroscopy (LIBS) Fundamentals and Applications* (Cambridge University Press, Cambridge, 2006)
3. R.E. Russo, X. Mao, H. Liu, J. Gonzalez, S.S. Mao, Talanta **57**, 425 (2002)
4. L. Van Vaeck, H. Struyf, W. Van Roy, F. Adams, Mass Spectrom. Rev. **13**, 189 (1994)
5. L. Van Vaeck, H. Struyf, W. Van Roy, F. Adams, Mass Spectrom. Rev. **13**, 209 (1994)
6. M. Karas, U. Bahr, U. Giessmann, Mass Spectrom. Rev. **10**, 335 (1991)
7. E. Betzig, J.K. Trautman, T.D. Harris, J.S. Weiner, R.L. Kostelak, Science **251**, 1468 (1991)
8. K. Dreisewerd, Chem. Rev. **103**, 395 (2003)
9. P.D. Setz, T.A. Schmitz, R. Zenobi, Rev. Sci. Instrum. **77**, 024101 (2006)
10. L. Kolaitis, D.M. Lubman, Anal. Chem. **58**, 2137 (1986)
11. V.V. Laiko, M.A. Baldwin, A.L. Burlingame, Anal. Chem. **72**, 652 (2000)
12. R.E. Russo, X. Mao, S.S. Mao, Anal. Chem. A **74**, 70 (2002)
13. L.V. Zhigilei, E. Leveugle, B.J. Garrison, Y.G. Yingling, M.I. Zeifman, Chem. Rev. **103**, 321 (2003)
14. S. Georgiou, A. Koubenakis, Chem. Rev. **103**, 349 (2003)
15. A. Vertes, P. Juhasz, M. De Wolf, R. Gijbels, Int. J. Mass Spectrom. Ion Proc. **94**, 63 (1989)
16. M. Karas, R. Kruger, Chem. Rev. **103**, 427 (2003)

17. N. Arnold, J. Gruber, J. Heitz, Appl. Phys. A **69**, S87 (1999)
18. S.B. Wen, X.L. Mao, R. Greif, R.E. Russo, J. Appl. Phys. **101**, 023114 (2007)
19. A. Bogaerts, Z. Chen, J. Anal. At. Spectrom. **19**, 1169 (2004)
20. A. Bogaerts, Z.Y. Chen, R. Gijbels, A. Vertes, Spectrochim. Acta, Part B **58**, 1867 (2003)
21. Z. Chen, A. Bogaerts, J. Appl. Phys. **97**, 063305 (2005)
22. G. Callies, P. Berger, H. Hugel, J. Phys. D **28**, 794 (1995)
23. F. Kokai, K. Takahashi, K. Shimizu, M. Yudasaka, S. Iijima, Appl. Phys. A **69**, S223 (1999)
24. S.S. Harilal, C.V. Bindhu, M.S. Tillack, F. Najmabadi, A.C. Gaeris, J. Appl. Phys. **93**, 2380 (2003)
25. S.B. Wen, X.L. Mao, R. Greif, R.E. Russo, J. Appl. Phys. **101**, 023115 (2007)
26. R. Hergenroder, Spectrochim. Acta, Part B **61**, 284 (2006)
27. J.M. Auerhammer, R. Walker, A.F.G. Van Der Meer, B. Jean, Appl. Phys. B **68**, 111 (1999)
28. I. Apitz, A. Vogel, Appl. Phys. A **81**, 329 (2005)
29. Z. Chen, A. Vertes, Phys. Rev. E **77**, 036316 (2008)
30. T.W. Heise, E.S. Yeung, Anal. Chem. **66**, 355 (1994)
31. J. Preisler, E.S. Yeung, Appl. Spectrosc. **49**, 1826 (1995)
32. J. Koch, S. Schlamp, T. Rosgen, D. Fliegel, D. Gunther, Spectrochim. Acta, Part B **62**, 20 (2007)
33. J. Koch, M. Walle, S. Schlamp, T. Rosgen, D. Gunther, Spectrochim. Acta, Part B **63**, 37 (2008)
34. H.C. Van De Hulst, *Light Scattering by Small Particles* (Dover, New York, 1981)
35. A.B. Brailovsky, S.V. Gaponov, V.I. Luchin, Appl. Phys. A **61**, 81 (1995)
36. X. Zhang, S.S. Chu, J.R. Ho, C.P. Grigoropoulos, Appl. Phys. A **64**, 545 (1997)
37. R. Hergenroder, J. Anal. At. Spectrom. **21**, 1016 (2006)
38. D.B. Geohegan, Appl. Phys. Lett. **60**, 2732 (1992)
39. S.S. Harilal, C.V. Bindhu, M.S. Tillack, F. Najmabadi, A.C. Gaeris, J. Phys. D **35**, 2935 (2002)
40. R. Kelly, A. Miotello, Nucl. Instrum. Methods Phys. Res. B **122**, 374 (1997)
41. Y.B. Zel'dovich, Y.P. Raizer, *Physics of Shock Waves and High-Temperature Hydrodynamic Phenomena* (Academic Press, New York, 1966)
42. L.I. Sedov, *Similarity and Dimensional Methods in Mechanics* (Academic Press, New York, 1959)
43. J.L. Taylor, Philos. Mag. **46**, 317 (1955)
44. P.E. Dyer, J. Sidhu, J. Appl. Phys. **64**, 4657 (1988)
45. S. Amoruso, J. Schou, J.G. Lunney, Appl. Phys. A **92**, 907 (2008)
46. C.S. Ake, R.S. De Castro, H. Sobral, M. Villagran-Muniz, J. Appl. Phys. **100**, 053305 (2006)
47. E.H. Piepmeier, H.V. Malmstadt, Anal. Chem. **41**, 700 (1969)
48. Y. Iida, Spectrochim. Acta, Part B **45**, 1353 (1990)
49. W. Sdorra, K. Niemax, Microchim. Acta **107**, 319 (1992)
50. X.L. Mao, W.T. Chan, M.A. Shannon, R.E. Russo, J. Appl. Phys. **74**, 4915 (1993)